Original Article

^{18}F-FAPI-42 PET/CT for preoperatively identifying intrahepatic cholangiocarcinoma and hepatocellular carcinoma

Ting Yang[1#], Yuan Yang[1,2#], Siqi Hu[1], Yujie Xie[1], Zijie Shen[1], Yong Zhang[1]

[1]Department of Nuclear Medicine, Third Affiliated Hospital of Sun Yat-sen University, Guangzhou, China; [2]Department of Nuclear Medicine, Zhujiang Hospital of Southern Medical University, Guangzhou, China

Contributions: (I) Conception and design: T Yang; (II) Administrative support: Y Zhang; (III) Provision of study materials or patients: T Yang, Y Yang, Y Xie; (IV) Collection and assembly of data: T Yang, Y Yang, Z Shen; (V) Data analysis and interpretation: T Yang, Y Yang, Y Zhang; (VI) Manuscript writing: All authors; (VII) Final approval of manuscript: All authors.

[#]These authors contributed equally to this work.

Correspondence to: Yong Zhang, MD. Department of Nuclear Medicine, Third Affiliated Hospital of Sun Yat-sen University, No. 600 Tianhe Road, Tianhe District, Guangzhou 510630, China. Email: zhangyn9@mail.sysu.edu.cn.

Background: Accurately differentiating hepatocellular carcinoma (HCC) from intrahepatic cholangiocarcinoma (ICC) is essential for therapeutic decision-making. This study aimed to explore the value of Fluor 18 (^{18}F)-conjugated fibroblast-activation protein inhibitor (FAPI-42) positron emission tomography-computed tomography (PET/CT) in distinguishing HCC from ICC preoperatively.

Methods: Patients with suspected intrahepatic lesions who underwent ^{18}F-FAPI-42 PET/CT were retrospectively assessed and placed into an HCC group and an ICC group based on postoperative pathology. Clinical indicators and PET/CT metabolic parameters were documented. Univariate and multivariate logistic regression analyses identified the independent predictive factors. The receiver operating characteristic curve and the area under the receiver operating curve (AUC) were used to determine the diagnostic efficacy.

Results: A total of 48 patients (age 55.4±10.8 years; 35 males and 13 females), including 28 in the HCC and 20 in the ICC group, were included. Univariate analysis revealed significant differences in clinical indicators such as gender, platelet count, and hepatitis B surface antigen, carbohydrate antigen 19-9 (CA19-9), and alpha fetoprotein (AFP) levels between the groups ($P<0.05$). Metabolic parameters including the maximum standardized uptake value (SUVmax), the total lesion-FAPI (TL-FAPI), and the target-to-background ratio (TBR) were statistically different between groups ($P<0.01$), and patients with ICC had higher values than those with HCC, while the FAPI tumor volume (FAPI-TV) was not statistically different ($P>0.05$). Multivariate binary logistic regression analysis identified the SUVmax ($P=0.003$) as an independent predictor for ICC, and the AUC of the regression-based diagnostic model for predicting ICC was 0.914 at an optimal cutoff value of 12.13, with a sensitivity of 85.0% and a specificity of 89.3%.

Conclusions: SUVmax is an independent predictor for ICC. With the optimal cutoff value of 12.13, ^{18}F-FAPI-42 PET/CT indicates good diagnostic efficacy in distinguishing between HCC and ICC.

Keywords: Fibroblast-activation protein inhibitor (FAPI); positron emission tomography-computed tomography (PET/CT); maximum standardized uptake value (SUVmax); hepatocellular carcinoma (HCC); intrahepatic cholangiocarcinoma (ICC)

Submitted Jul 24, 2024. Accepted for publication Nov 08, 2024. Published online Dec 18, 2024.
doi: 10.21037/qims-24-1489
View this article at: https://dx.doi.org/10.21037/qims-24-1489

Introduction

Two common types of primary liver cancer are hepatocellular carcinoma (HCC) and intrahepatic cholangiocarcinoma (ICC), accounting for 75–85% and 10–15% of liver cancer cases, respectively (1). Compared to HCC, ICC is highly invasive with no effective chemotherapy and typically requires extensive liver resection, including resection of tumor-invading blood vessels, bile ducts, and adjacent tissues. Even with radical surgical resection, the 5-year overall survival (OS) is only 20–35% (2). The incidence rate of ICC has been rising in recent years (3). Given that HCC and ICC have significantly different biological behaviors, preferred therapeutic decisions, and prognoses, preoperatively distinguishing between them is critical to clinical decision-making. Carbohydrate antigen 19-9 (CA19-9) is considered to be an effective blood biomarker in clinical practice for distinguishing between HCC carcinoma and ICC. However, a large number of studies have indicated that the actual diagnostic accuracy of CA19-9 is not ideal, with a sensitivity and specificity of approximately 50–70% and 70–80%, respectively, along with a high misdiagnosis rate and missed diagnosis rate (4,5). Noninvasive preoperative imaging of ICC mainly includes contrast computed tomography (CT), magnetic resonance imaging (MRI), and positron emission tomography/CT (PET/CT) (6). MRI is the preferred method for differentiating HCC from ICC, which can better visualize the enhancement of the lesion. Fluorodeoxyglucose ^{18}F (^{18}F-FDG) PET/CT is useful for the diagnosis of various solid tumors (7). Semiquantitative parameters of FDG PET/CT can reflect the metabolic activity of the tumor. Although FDG PET/CT has unique advantages in the staging of solid tumors, its performance in the diagnosis and differential diagnosis of liver cancers is unsatisfactory.

Fibroblast-activation protein (FAP) is a type of II transmembrane serine protease belonging to the proline oligopeptidase family and shows favorable pharmacokinetics and biodistribution *in vivo* (8). FAP is highly expressed in various tumor-associated fibroblasts, especially epithelial tumors, but not in normal tissues or benign tumor stroma, making it a key target in the diagnosis and treatment of malignant tumors. FAP inhibitor (FAPI), a newly discovered reagent for targeting the tumor microenvironment (TME), enables visualization of cancer-associated fibroblasts (CAFs) *in vivo* and shows promising applications in the noninvasive assessment of tumors (9). Previous studies have demonstrated the superior performance of FAPI PET/CT compared to FDG in liver cancers, with both HCC and ICC exhibiting high uptake of FAPI (10), as FAPI is not dependent on glucose activity and has a significantly reduced physiological uptake into the liver. Recently, it has been found that FAP expression is higher in ICC than in HCC (11), which suggests that FAPI PET/CT may be used to clinically differentiate these two subtypes and guide the surgical planning. In addition, the related volumetric parameters of FAPI PET/CT have not been adequately clarified, and there remains a lack of quantitative analysis and research regarding the use of FAPI PET/CT in distinguishing between different pathologic types.

Our study thus aimed to investigate the value of ^{18}F-FAPI-42 PET/CT imaging in differentiating HCC from ICC in conjunction with common clinical indicators. The optimal parameters for differentiation were also determined. Since ^{18}F provides higher yield, energy, and resolution than does ^{68}Ga, we sought to clarify the value of ^{18}F-FAPI-42 PET/CT in the preoperative identification of HCC and ICC. We present this article in accordance with the STROBE reporting checklist (available at https://qims.amegroups.com/article/view/10.21037/qims-24-1489/rc).

Methods

Study design

In this retrospective study, we evaluated the semiquantitative parameters obtained by ^{18}F-FAPI-42 PET/CT as a preoperative imaging indicator for discriminating between HCC and ICC. This study was conducted in accordance with the Declaration of Helsinki (as revised in 2013) and was approved by the Ethics Committee of The Third Affiliated Hospital of Sun Yat-sen University (No. II2023-060). The requirement for individual consent was waived due to the retrospective nature of the analysis.

Patients

Patients with suspected hepatic tumors who underwent ^{18}F-FAPI-42 PET/CT preoperatively between March 2021 and January 2023 were identified from the institutional database. Patients were included if they satisfied the following criteria: (I) completion of ^{18}F-FAPI-42 PET/CT within 1 month before surgery; (II) pathologically confirmed primary HCC or ICC; and (III) available clinical data. Meanwhile, patients were excluded if they met any of

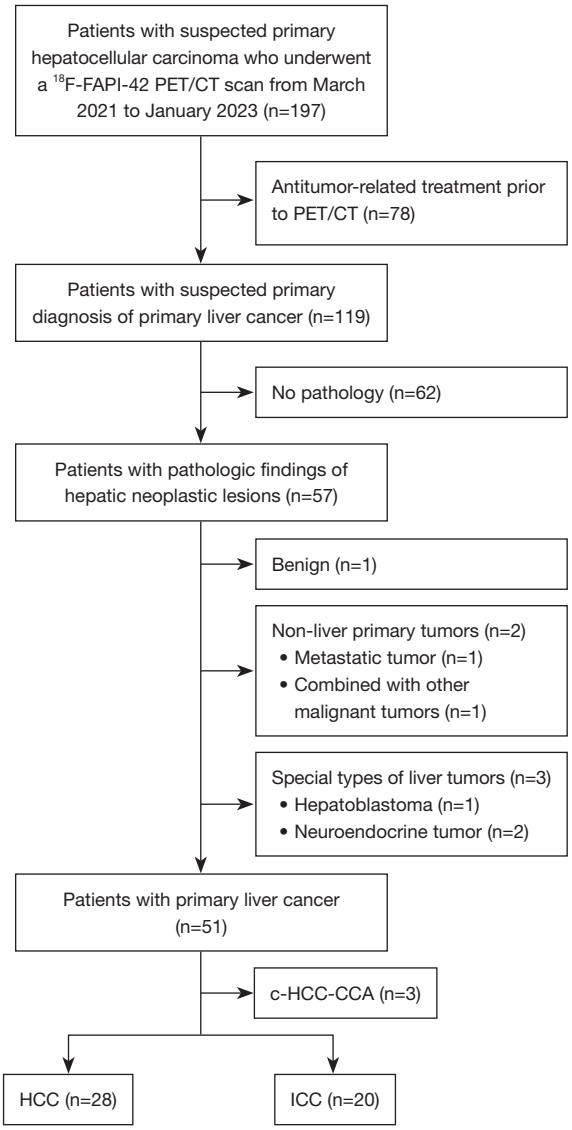

Figure 1 Flowchart of patient selection. ^{18}F-FAPI-42 PET/CT, Fluor 18 (^{18}F)-conjugated fibroblast-activation protein inhibitor (FAPI-42) positron emission tomography-computed tomography; HCC, hepatocellular carcinoma; ICC, intrahepatic cholangiocarcinoma; c-HCC-CCA, combined hepatocellular-cholangiocarcinoma.

the following criteria: (I) incomplete clinical and pathologic information; (II) types of liver cancers other than HCC or ICC; and (III) a negative imaging result on PET/CT or an unclear boundary of the hepatic lesion precluding delineation via PET volume computer-assisted reading (VCAR) software. The flowchart of patient selection is displayed in *Figure 1*.

Data collection

The clinical data collected included were age, gender, hepatitis B virus (HBV) infection, platelet count (PLT), gamma-glutamyl transpeptidase (GGT), alanine transaminase (ALT), aspartate transaminase (AST), albumin (ALB), and total bilirubin (TBIL) levels, and preoperative serum CA19-9 and alpha fetoprotein (AFP) levels. In addition, we recorded the pathological information of the patient, including the tissue type and the degree of differentiation.

PET/CT imaging and analysis

^{18}F-FAPI-42 was provided by Guangdong Huixuan Pharmaceutical Technology Co. Ltd. (Guangzhou, China). No special preparation was required before scanning. Patients underwent ^{18}F-FAPI PET/CT via a Discovery Elite device (GE HealthCare, Chicago, IL, USA) while lying in a supine position, with an injection volume of 2.96–5.19 MBq (0.08–0.14 mCi)/kg. Scanning was performed 60 minutes after injection. Following non–contrast-enhanced CT (120 keV and 120 mA), PET was acquired in the 3D mode with a scanning range covering skull base to the midfemur (2–4 minutes/bed; 7–9 beds). PET/CT scans were evaluated independently by two experienced nuclear medicine physicians (T.Y. and Y.Z.). Discrepancies were resolved via concurrent reading. PET VCAR software (GE HealthCare) was used to delineate the regions of interest (ROIs) of the intrahepatic lesion in transaxial slices and to automatically adapt them to a 3D volume. The system automatically calculates the maximum standardized uptake value (SUVmax) and the mean standardized uptake value (SUVmean) of the lesion, and uses the relative threshold method, with 40% of SUVmax as the threshold. For patients with multiple lesions, only the lesion with the highest FAPI uptake (SUVmax) was enrolled for analysis, which was matched with the gross pathological specimen based on location and size. The software automatically divided the lesion to obtain the corresponding volume parameter FAPI tumor volume (FAPI-TV), from which the parameter total lesion-FAPI (TL-FAPI) was calculated as follows: TL-FAPI = SUVmean × FAPI-TV. For multiple liver lesions, only the lesion with the highest uptake was measured and included in statistical analysis. The SUVmean of the normal liver was measured in the 3-cm^2 area surrounding the location of liver tissue, with the areas such as focal changes of fatty liver, major vessels and bile ducts, and liver surface margins being

avoided. Meanwhile, the target-to-background ratio (TBR) of the lesion was calculated as follows: TBR = SUVmax of the lesion/SUVmean of normal liver tissue.

Statistical analysis

Continuous variables are represented as the mean and standard deviation or as the median with the interquartile range (IQR) if they were not normally distributed. The Student's *t*-test or Mann-Whitney test was performed to analyze the differences between the two groups. The Chi-squared test or Fisher exact test was used to compare the frequencies of categorical variables between HCC and ICC. Univariate and multivariate analyses were used to identify independent the predictive factors for ICC. Receiver operating characteristic (ROC) curves were used to identify the threshold of continuous variables in the identification ICC. The sensitivity and specificity were obtained using an optimal cutoff with the maximum Youden index. A two-sided P value <0.05 was considered indicative of a statistically significant difference. All data were analyzed using SPSS 26 (IBM Corp., Armonk, NY, USA).

Results

Patient characteristics

This study ultimately included 48 patients (age 55.4±10.8 years; 35 males and 13 females), including 28 patients with HCC and 20 patients with ICC. The patient's characteristics are summarized in *Table 1*. The clinical indicators included age, gender, HBV infection, AST, ALT, glutamine transpeptidase, albumin, total bilirubin, serum AFP, and CA19-9 levels, PLT count, tumor size, and clinical stage. The HCC and ICC groups differed significantly in terms of gender (P=0.018), platelet count (P=0.002), HBV infection (P<0.001), CA19-9 level (P=0.001), and AFP level (P<0.001). The proportion of male patients was greater in the HCC group than in the ICC group (24/28 *vs.* 11/20), as was the proportion of patients with HBV infection. Meanwhile, patients in the ICC group had higher levels of PLT and CA19-9. There were no statistically significant differences between the two groups for the other indicators, including age, AST, ALT, glutamine transpeptidase, albumin, total bilirubin, tumor size, and clinical stage (all P values >0.05).

PET/CT semiquantitative parameters

The parameters SUVmax, FAPI-TV, and TL-FAPI were all automatically calculated by the PET VCAR software (*Figure 2*). The ICC groups had significantly higher SUVmax (P<0.001), TL-FAPI (P=0.008), and TRB (P<0.001) as compared to the HCC group, while there was no statistical difference in FAPI-TV (P=0.217) (*Table 2*). The SUVmax in the HCC group and the ICC group was 8.04±3.87 and 18.81±8.17, respectively (P<0.001). The representative PET/CT images for both HCC and ICC are shown in *Figure 3*.

Multifactor logistic regression analysis

The statistically significant indicators in the univariate analysis (gender, platelet count, HBV infection, SUVmax, TL-FAPI, and serum CA19-9 and AFP levels) were included in the multifactor logistic regression (*Table 3*). The independent predictors for distinguishing between ICC and HCC were platelet count [odds ratio (OR) =1.022; 95% confidence interval (CI): 1.001–1.044; P=0.041] and SUVmax (OR =1.593; 95% CI: 1.172–2.165; P=0.003). The cutoff value of SUVmax for diagnosing ICC was 12.13, with a sensitivity of 85.0% and a specificity of 89.3%. The plotted ROC curve is shown in *Figure 4*, and the area under the curve (AUC) was 0.914.

Discussion

Due to the significant differences in treatment and prognosis between HCC and ICC, noninvasive imaging methods bear considerable clinical relevance in distinguishing between the two and can help avoid invasive tissue biopsy and surgery-related complications (12). Enhanced CT and MRI are recommended to differentiate HCC and ICC. HCC is a highly vascular tumor supplied by the hepatic artery, and its typical enhancement feature as fast in and out (13). ICC is a hypovascular tumor rich in fibrous tissue, which mainly manifests as progressive delayed enhancement, mild enhancement at the edge of the arterial phase, and significant enhancement in the delayed phase (14). PET/CT imaging plays an important role in the comprehensive management of hepatocellular tumors (15,16). ^{18}F-FDG PET/CT or PET/MR can help differentiate between HCC and ICC to some extent given the differences in glucose uptake and glycolysis mechanisms between the two,

Table 1 Clinical characteristics of patients with HCC and ICC

Clinical feature	HCC (n=28)	ICC (n=20)	P value
Gender			0.018*
Male	24 (85.7)	11 (55.0)	
Female	4 (14.3)	9 (45.0)	
Age (years)	54.46±9.93	56.80±12.15	0.468
AST (U/L)	45 [62]	30 [44]	0.30
ALT (U/L)	34.5 [56]	21.5 [34]	0.181
GGT (IU/L)	83.5 [169]	76.5 [174]	0.291
ALB (g/L)	38.8±5.81	39.17±5.45	0.821
TBIL (μmol/L)	10.9 [7]	11.45 [8]	0.645
PLT (G/L)	153.07±62.46	242.45±107.27	0.002*
HBsAg infection			<0.001*
(–)	5 (17.9)	14 (70.0)	
(+)	23 (82.1)	6 (30.0)	
CA19-9 (U/mL)			0.001*
≤37	25 (89.3)	8 (40.0)	
>37	3 (10.7)	12 (60.0)	
AFP (ng/mL)			<0.001*
≤20	10 (35.7)	19 (95.0)	
>20	18 (64.3)	1 (5.0)	
Tumor size (mm)			
Maximum	54.53±29.86	69.30±32.05	0.113
Minimum	44.53±25.89	51.49±19.83	0.327
Clinical staging			0.158
I	9	3	
II	2	1	
III	8	4	
IV	9	12	

Normally distributed continuous variables are represented as the mean ± standard deviation; nonnormally distributed continuous variables are represented as the median [interquartile range]; categorical variables are represented as the number of cases (percentage). *, P<0.05. HCC, hepatocellular carcinoma; ICC, intrahepatic cholangiocarcinoma; AST, aspartate transaminase; ALT, alanine transaminase; GGT, gamma-glutamyl transpeptidase; ALB, albumin; TBIL, total bilirubin; PLT, platelet; CA19-9, carbohydrate antigen 19-9; AFP, alpha fetoprotein.

especially for lumpy intrahepatic cholangiocarcinoma, but its diagnostic efficacy is not satisfactory (17,18). Moreover, there are recognized limitations to the use of ^{18}F-FDG PET/CT in liver diseases, including a high physiologic uptake of glucose by normal liver tissue, a low uptake in well-differentiated primary hepatocellular tumors, and an insufficient TBR, restricting its utility in the diagnosis and differential diagnosis of primary HCC.

FAPI is a novel reagent for targeting the TME and observing CAFs *in vivo*, demonstrating promising applications in the noninvasive evaluation of tumors. In Chen *et al.*'s study (19), the physiological uptake of FAPI

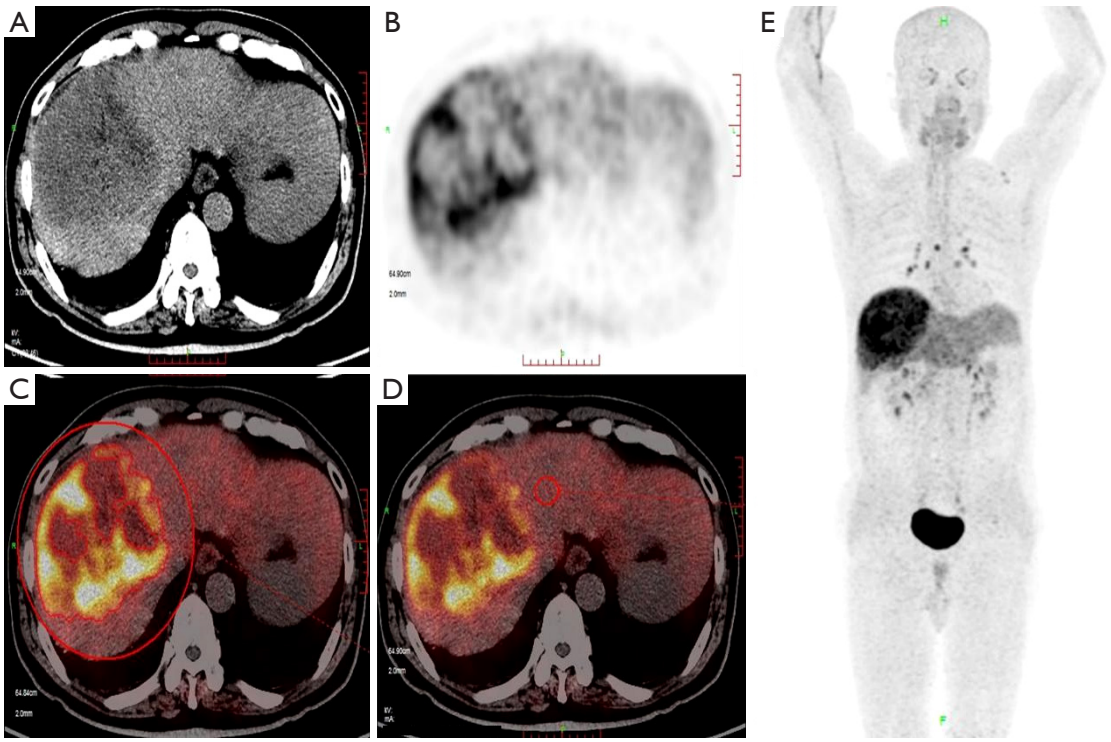

Figure 2 ROI of the liver tumor and normal liver tissue in ^{18}F-FAPI-42 PET/CT. (A,B) The axial images of CT and PET. (C,D) Fusion PET/CT images for the ROI of hepatic lesions obtained with the three-dimensional sketching method (the bigger red circle) and the ROI of normal liver parenchyma (the smaller red circle) using the fixed area method (area of 3 cm^2). Semiquantitative parameters were obtained automatically. (E) The maximal intensity projection image. ROI, region of interest; ^{18}F-FAPI-42 PET/CT, Fluor 18 (^{18}F)-conjugated fibroblast-activation protein inhibitor (FAPI-42) positron emission tomography-computed tomography; CT, computed tomography; PET, positron emission tomography.

Table 2 Comparison of the PET/CT characteristics between HCC and ICC

PET/CT parameter	HCC	ICC	P value
SUVmax	8.04±3.87	18.81±8.17	<0.001*
FAPI-TV (cm^3)	32.29 (17.74–127.51)	82.45 (22.79–185.19)	0.217
TL-FAPI (g)	141.72 (51.60–742.71)	452.56 (209.26–1,892.80)	0.008*
TRB	5.76 (3.94–8.82)	16.41 (9.58–18.95)	<0.001*

Normally distributed continuous variables are represented as mean ± standard deviation; nonnormally distributed continuous variables are represented as median (interquartile range). *, P<0.05. PET/CT, positron emission tomography-computed tomography; HCC, hepatocellular carcinoma; ICC, intrahepatic cholangiocarcinoma; SUVmax, maximum standardized uptake value; FAPI-TV, fibroblast activation protein inhibitor tumor volume; TL-FAPI, total amount of tumor fibroblast activation protein expression; TBR, target-to-background ratio.

was low in normal liver tissue, and hepatic malignant tumors had a much higher uptake of FAPI than did normal liver tissue, presenting a prominent TBR that enabled them to be distinguished from normal liver tissue. In recent years, studies have suggested that the expression of FAP in ICC tends to be higher than that in HCC (19). The semiquantitative parameters of FAPI PET/CT may help to distinguish between the pathological types of primary liver cancer, but there are currently few relevant reports in the literature. We thus conducted this study to assess the clinical value of ^{18}F-FAPI-42 PET/CT in the differential diagnosis of HCC and ICC.

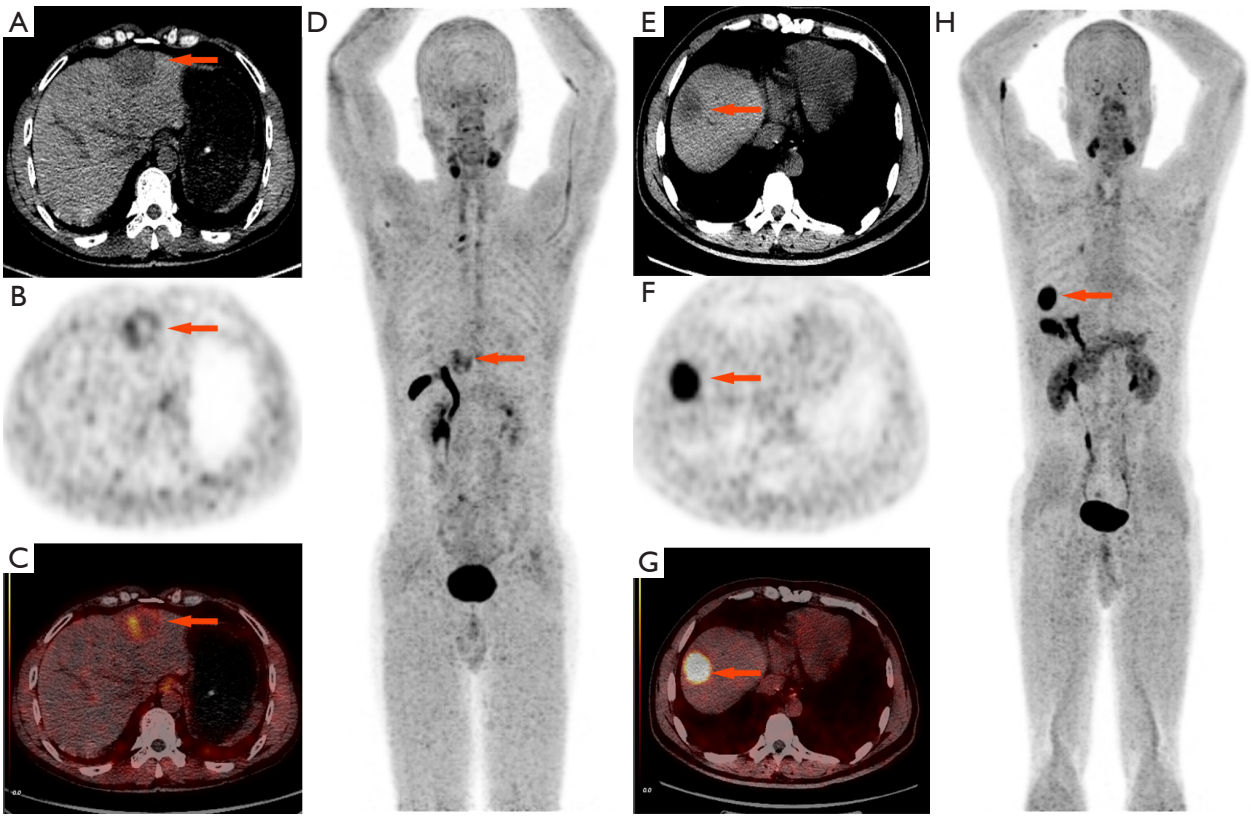

Figure 3 Representative images for both HCC and ICC. (A) Transaxial CT, (B) transaxial PET, (C) transaxial fusion PET/CT, and (D) MIP (anterior view) in a 48-year-old man patient with HCC; the mass was in his hepatic II segment (arrow), its size was about 4.0 cm × 3.8 cm, and the SUVmax was 4.1. (E) Transaxial CT, (F) transaxial PET, (G) transaxial fusion PET/CT, and (H) MIP (anterior view) in a 50-year-old man with ICC. The mass (arrow) was about 3.5 cm × 3.2 cm, with significantly increased FAPI uptake (SUVmax =14.9). HCC, hepatocellular carcinoma; ICC, intrahepatic cholangiocarcinoma; CT, computed tomography; PET, positron emission tomography; MIP, maximum intensity projection; SUVmax, maximum standardized uptake value; FAPI, fibroblast activation protein inhibitor.

Table 3 Multivariable logistic regression analyses for the differentiation of ICC from HCC

Variable	B	OR	P value	95% CI of OR
SUVmax	0.466	1.593	0.003	(1.172–2.165)
PLT	0.022	1.022	0.041	(1.001–1.044)

ICC, intrahepatic cholangiocarcinoma; HCC, hepatocellular carcinoma; SUVmax, maximum standardized uptake value; PLT, platelet.

Our study included 48 patients, 28 with HCC and 20 with ICC. There was no statistically significant difference in age, tumor size, or clinical staging between the two groups (P>0.05), indicating a certain degree of comparability. Univariate analysis showed that gender, platelet count, hepatitis B surface antigen level, AFP level, and CA19-9 level were statistically different between the HCC and ICC group (P<0.05). Tumor markers AFP and CA19-9 may help distinguish between ICC and HCC since elevated AFP level (>20 ng/mL) was more common in the HCC group (P<0.001) while elevated CA19-9 level (>37 U/mL) was more common in the ICC group (P=0.001); however, it should be noted that their sensitivity in distinguishing between the two was not high (64.3% and 60.0%, respectively). Previous studies have indicated that tumor cells promote the activation and aggregation of platelets by secreting a variety of active substances, such as adenosine diphosphate (ADP) and matrix metalloproteinase-2 (MMP-2) (20,21). Activated platelets participate in and regulate tumor growth in a variety of ways (22). In our study, ICC had a higher platelet count than did HCC (P=0.002), which is consistent with previous research (23).

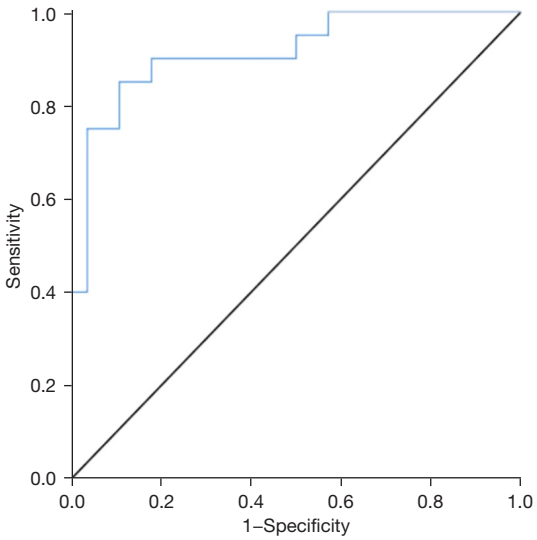

Figure 4 ROC curves of the SUVmax parameters for differentiating HCC from ICC. The area under the curve is 0.914, and the cutoff value of SUVmax for diagnosing intrahepatic cholangiocarcinoma is 12.13, with a sensitivity and specificity of 85% and 89.3%, respectively. ROC, receiver operating characteristic; SUVmax, maximum standard uptake value; HCC, hepatocellular carcinoma; ICC, intrahepatic cholangiocarcinoma.

In the multivariate logistic regression analysis, platelet count was found to be an independent predictor of ICC, but the AUC was only 0.752. The higher platelet count of ICC contributes to its highly invasive biological characteristics and poor prognosis.

Among the semiquantitative parameters of FAPI PET/CT, FAPI-TV showed no significant difference between the HCC and ICC groups (P=0.217), while TL-FAPI was significantly different (P=0.008), indirectly indicating that the FAP expression level differs considerably between HCC and ICC. In the univariate analysis, SUVmax, TL-FAPI, and TRB were significantly higher in ICC than in HCC (P<0.001). In the multivariate analysis, SUVmax emerged as an independent predictor of ICC: at an optimal cutoff value of 12.13, the AUC was 0.914. This suggests that SUVmax has good diagnostic efficacy in distinguishing ICC from HCC, with a diagnostic sensitivity of 85.0% and a specificity of 89.3%.

Although both HCC and ICC exhibited a high uptake of FAPI (SUVmax =8 *vs.* 19), their mechanisms and expression patterns are not entirely the same (10). There is growing evidence indicating the presence of cross-talk between tumor cells and the peritumoral stroma in a variety of malignancies. Chronic liver injury, inflammation, and fibrosis play a key role in the development of HCC but a small role in ICC (10). The development of ICC has not yet been fully examined, and it is not yet clear whether the activation of certain pathways in the premalignant environment (PME) can promote the development of ICC, or whether it mainly occurs after tumor formation. However, most of the recent research suggests that fibrosis is not strongly associated with the development of ICC cancer but rather leads to strong reactive connective tissue formation after tumor occurrence (24). The TME develops and coevolves in already-formed tumors, playing a crucial role in both ICC and HCC (25,26). In the TME, the collagenolytic effect of FAP promotes tumor growth and invasion. ICC is a highly invasive malignant tumor derived from the bile duct epithelium. As with other ductal malignant tumors such as pancreatic cancer, the most prominent feature is the presence of rich mesenchymal matrix in connective tissue, which is low-vascularized (27). The tumor tissue is surrounded by a highly demyelinated stoma which is poor in vascularity but rich in CAFs. The number of CAFs even far exceeds the actual cholangiocarcinoma cells number, expressing higher levels of FAPs. Previous studies suggest that the strong demyelination response in cholangiocarcinoma may be related to the high expression of platelet-derived growth factor D (PDGF-D) in cholangiocarcinoma cells, which plays a crucial role in promoting the activation and recruitment of cancer-related fibroblasts (28). Shi *et al.* (29) analyzed the expression of FAP in liver tumor tissues through immunohistochemical staining, and the results also suggested that the stromal cells of ICC had greater FAP expression than did the stromal cells of HCC. Therefore, we believe that ^{18}F-FAPI-42 PET/CT can effectively differentiate HCC from ICC, with SUVmax being an independent predictor of ICC. The large accumulation of FAPI is not consistent with the anatomical location of the CT scan, which may be related to the considerable spatial heterogeneity of the morphological features of the tissues within the tumor and the complexity of the tumor biology.

We unexpectedly found differences in liver background uptake between the patient groups. We speculate that this may be related to the degree of hepatic fibrosis in the patients. The liver background uptake was higher in patients with a high degree of liver fibrosis than in those with a low degree of liver fibrosis, which is in line with another study (30). This may be because FAP is not expressed in normal hepatocytes and is highly expressed in activated

stellate cells and fibroblasts. FAP expression is induced by lymphocyte- or macrophage-derived cytokines such as TNFα, MCP1, and IL6 (31), and an increase in the number of FAP-expressing fibroblasts correlates with the histologic severity of fibrosis (32). In addition, we observed tubular radiotracer uptake in the liver/porta hepatis, which may be related to intense FAPI uptake caused by cholangitis.

The study involved several limitations which should be acknowledged. First, we employed a single-center design, with a relatively small patient size, and thus larger, multicenter, prospective studies are needed for further validation. Second, the pathological results of some cases were confirmed with a puncture biopsy sample and not with the entire surgical specimen. The results of puncture biopsy cannot fully reflect the overall appearance of the lesion. Third, the value of SUVmax may overlap with other types of tumors or benign hepatic lesions.

Conclusions

^{18}F-FAPI-42 PET/CT can effectively distinguish between HCC and ICC, with the SUVmax being an independent predictor.

Acknowledgments

The authors sincerely thank all participants for their cooperation and the technicians for the FAPI radiolabeling and PET/CT scans.
Funding: None.

Footnote

Reporting Checklist: The authors have completed the STROBE reporting checklist. Available at https://qims.amegroups.com/article/view/10.21037/qims-24-1489/rc

Conflicts of Interest: All authors have completed the ICMJE uniform disclosure form (available at https://qims.amegroups.com/article/view/10.21037/qims-24-1489/coif). The authors have no conflicts of interest to declare.

Ethical Statement: The authors are accountable for all aspects of the work in ensuring that questions related to the accuracy or integrity of any part of the work are appropriately investigated and resolved. This study was conducted according to the Declaration of Helsinki (as revised in 2013) and was approved by the ethics committee of The Third Affiliated Hospital of Sun Yat-sen University (No. II2023-060). The requirement for individual consent was waived due to the retrospective nature of the analysis.

References

1. Sung H, Ferlay J, Siegel RL, Laversanne M, Soerjomataram I, Jemal A, Bray F. Global Cancer Statistics 2020: GLOBOCAN Estimates of Incidence and Mortality Worldwide for 36 Cancers in 185 Countries. CA Cancer J Clin 2021;71:209-49.
2. Zhang XF, Beal EW, Bagante F, Chakedis J, Weiss M, Popescu I, Marques HP, Aldrighetti L, Maithel SK, Pulitano C, Bauer TW, Shen F, Poultsides GA, Soubrane O, Martel G, Koerkamp BG, Itaru E, Pawlik TM. Early versus late recurrence of intrahepatic cholangiocarcinoma after resection with curative intent. Br J Surg 2018;105:848-56.
3. An L, Zheng R, Zhang S, Chen R, Wang S, Sun K, Lu L, Zhang X, Zhao H, Zeng H, Wei W, He J. Hepatocellular carcinoma and intrahepatic cholangiocarcinoma incidence between 2006 and 2015 in China: estimates based on data from 188 population-based cancer registries. Hepatobiliary Surg Nutr 2023;12:45-55.
4. Liang B, Zhong L, He Q, Wang S, Pan Z, Wang T, Zhao Y. Diagnostic Accuracy of Serum CA19-9 in Patients with Cholangiocarcinoma: A Systematic Review and Meta-Analysis. Med Sci Monit 2015;21:3555-63.
5. Izquierdo-Sanchez L, Lamarca A, La Casta A, Buettner S, Utpatel K, Klümpen HJ, et al. Cholangiocarcinoma landscape in Europe: Diagnostic, prognostic and therapeutic insights from the ENSCCA Registry. J Hepatol 2022;76:1109-21.
6. Roberts LR, Sirlin CB, Zaiem F, Almasri J, Prokop LJ, Heimbach JK, Murad MH, Mohammed K. Imaging for the diagnosis of hepatocellular carcinoma: A systematic review and meta-analysis. Hepatology 2018;67:401-21.
7. Sacks A, Peller PJ, Surasi DS, Chatburn L, Mercier G,

Subramaniam RM. Value of PET/CT in the management of primary hepatobiliary tumors, part 2. AJR Am J Roentgenol 2011;197:W260-5.
8. Loktev A, Lindner T, Mier W, Debus J, Altmann A, Jäger D, Giesel F, Kratochwil C, Barthe P, Roumestand C, Haberkorn U. A Tumor-Imaging Method Targeting Cancer-Associated Fibroblasts. J Nucl Med 2018;59:1423-9.
9. Kratochwil C, Flechsig P, Lindner T, Abderrahim L, Altmann A, Mier W, Adeberg S, Rathke H, Röhrich M, Winter H, Plinkert PK, Marme F, Lang M, Kauczor HU, Jäger D, Debus J, Haberkorn U, Giesel FL. (68)Ga-FAPI PET/CT: Tracer Uptake in 28 Different Kinds of Cancer. J Nucl Med 2019;60:801-5.
10. Affo S, Yu LX, Schwabe RF. The Role of Cancer-Associated Fibroblasts and Fibrosis in Liver Cancer. Annu Rev Pathol 2017;12:153-86.
11. Shi X, Xing H, Yang X, Li F, Yao S, Congwei J, Zhao H, Hacker M, Huo L, Li X. Comparison of PET imaging of activated fibroblasts and (18)F-FDG for diagnosis of primary hepatic tumours: a prospective pilot study. Eur J Nucl Med Mol Imaging 2021;48:1593-603.
12. Zhang N, Li Y, Zhao M, Chang X, Tian F, Qu Q, He X. Sarcomatous intrahepatic cholangiocarcinoma: Case report and literature review. Medicine (Baltimore) 2018;97:e12549.
13. Gao R, Zhao S, Aishanjiang K, Cai H, Wei T, Zhang Y, Liu Z, Zhou J, Han B, Wang J, Ding H, Liu Y, Xu X, Yu Z, Gu J. Deep learning for differential diagnosis of malignant hepatic tumors based on multi-phase contrast-enhanced CT and clinical data. J Hematol Oncol 2021;14:154.
14. Huang B, Wu L, Lu XY, Xu F, Liu CF, Shen WF, Jia NY, Cheng HY, Yang YF, Shen F. Small Intrahepatic Cholangiocarcinoma and Hepatocellular Carcinoma in Cirrhotic Livers May Share Similar Enhancement Patterns at Multiphase Dynamic MR Imaging. Radiology 2016;281:150-7.
15. Jiang C, Zhao L, Xin B, Ma G, Wang X, Song S. (18) F-FDG PET/CT radiomic analysis for classifying and predicting microvascular invasion in hepatocellular carcinoma and intrahepatic cholangiocarcinoma. Quant Imaging Med Surg 2022;12:4135-50.
16. Hu S, Xie Y, Yang T, Yang Y, Zou Q, Jiao J, Zhang Y. Tumor metabolism derived from (18)F-FDG PET/CT in predicting the macrotrabecular-massive subtype of hepatocellular carcinoma. Quant Imaging Med Surg 2023;13:309-19.
17. Lee JD, Yang WI, Park YN, Kim KS, Choi JS, Yun M, Ko D, Kim TS, Cho AE, Kim HM, Han KH, Im SS, Ahn YH, Choi CW, Park JH. Different glucose uptake and glycolytic mechanisms between hepatocellular carcinoma and intrahepatic mass-forming cholangiocarcinoma with increased (18)F-FDG uptake. J Nucl Med 2005;46:1753-9.
18. Çelebi F, Yaghouti K, Cindil E, Dogusoy GB, Tokat Y, Balcı C. The Role of 18F-FDG PET/MRI in the Assessment of Primary Intrahepatic Neoplasms. Acad Radiol 2021;28:189-98.
19. Chen H, Pang Y, Wu J, et al. Comparison of [68Ga] Ga-DOTA-FAPI-04 and [18F] FDG PET/CT for the diagnosis of primary and metastatic lesions in patients with various types of cancer. Eur J Nucl Med Mol Imaging 2020;47:1820-32.
20. Jurasz P, Sawicki G, Duszyk M, Sawicka J, Miranda C, Mayers I, Radomski MW. Matrix metalloproteinase 2 in tumor cell-induced platelet aggregation: regulation by nitric oxide. Cancer Res 2001;61:376-82.
21. Jurasz P, Alonso-Escolano D, Radomski MW. Platelet--cancer interactions: mechanisms and pharmacology of tumour cell-induced platelet aggregation. Br J Pharmacol 2004;143:819-26.
22. Best MG, Sol N, Kooi I, Tannous J, Westerman BA, Rustenburg F, et al. RNA-Seq of Tumor-Educated Platelets Enables Blood-Based Pan-Cancer, Multiclass, and Molecular Pathway Cancer Diagnostics. Cancer Cell 2015;28:666-76.
23. Zhang X, Huang WJ, Zhang ML, Wang W, Niu Y, Wang RT, Liu ZY. Utility of mean platelet volume in differentiating intrahepatic cholangiocarcinoma from hepatocellular carcinoma. BMC Gastroenterol 2022;22:288.
24. Montori M, Scorzoni C, Argenziano ME, Balducci D, De Blasio F, Martini F, Buono T, Benedetti A, Marzioni M, Maroni L. Cancer-Associated Fibroblasts in Cholangiocarcinoma: Current Knowledge and Possible Implications for Therapy. J Clin Med 2022;11:6498.
25. Sirica AE. The role of cancer-associated myofibroblasts in intrahepatic cholangiocarcinoma. Nat Rev Gastroenterol Hepatol 2011;9:44-54.
26. Baglieri J, Brenner DA, Kisseleva T. The Role of Fibrosis and Liver-Associated Fibroblasts in the Pathogenesis of Hepatocellular Carcinoma. Int J Mol Sci 2019;20:1723.
27. Sirica AE, Gores GJ, Groopman JD, Selaru FM, Strazzabosco M, Wei Wang X, Zhu AX. Intrahepatic Cholangiocarcinoma: Continuing Challenges and Translational Advances. Hepatology 2019;69:1803-15.
28. Cadamuro M, Nardo G, Indraccolo S, Dall'olmo L,

Sambado L, Moserle L, Franceschet I, Colledan M, Massani M, Stecca T, Bassi N, Morton S, Spirli C, Fiorotto R, Fabris L, Strazzabosco M. Platelet-derived growth factor-D and Rho GTPases regulate recruitment of cancer-associated fibroblasts in cholangiocarcinoma. Hepatology 2013;58:1042-53.
29. Shi X, Xing H, Yang X, Li F, Yao S, Zhang H, Zhao H, Hacker M, Huo L, Li X. Fibroblast imaging of hepatic carcinoma with (68)Ga-FAPI-04 PET/CT: a pilot study in patients with suspected hepatic nodules. Eur J Nucl Med Mol Imaging 2021;48:196-203.
30. Guo W, Pang Y, Yao L, et al. Imaging fibroblast activation protein in liver cancer: a single-center post hoc retrospective analysis to compare [68Ga]Ga-FAPI-04 PET/CT versus MRI and [18F]-FDG PET/CT. Eur J Nucl Med Mol Imaging 2021;48:1604-17.
31. Yang AT, Kim YO, Yan XZ, Abe H, Aslam M, Park KS, Zhao XY, Jia JD, Klein T, You H, Schuppan D. Fibroblast Activation Protein Activates Macrophages and Promotes Parenchymal Liver Inflammation and Fibrosis. Cell Mol Gastroenterol Hepatol 2023;15:841-67.
32. Levy MT, McCaughan GW, Marinos G, Gorrell MD. Intrahepatic expression of the hepatic stellate cell marker fibroblast activation protein correlates with the degree of fibrosis in hepatitis C virus infection. Liver 2002;22:93-101.

Cite this article as: Yang T, Yang Y, Hu S, Xie Y, Shen Z, Zhang Y. ^{18}F-FAPI-42 PET/CT for preoperatively identifying intrahepatic cholangiocarcinoma and hepatocellular carcinoma. Quant Imaging Med Surg 2025;15(1):741-751. doi: 10.21037/qims-24-1489

